A Multi-Timescale Map of Radiative and Nonradiative Decay Pathways for Excitons in CdSe Quantum Dots

Kathryn E. Knowles, Eric A. McArthur, and Emily A. Weiss*

Department of Chemistry, Northwestern University, 2145 Sheridan Road, Evanston, Illinois 60628-3113, United States

ABSTRACT A combination of transient absorption (TA) and time-resolved photoluminescence (TRPL) spectroscopies performed on solution-phase samples of colloidal CdSe quantum dots (QDs) allows the construction of a time-resolved, charge carrier-resolved map of decay from the first excitonic state of the QD. Data from TA and TRPL yield the same six exponential components, with time constants ranging from ~1 ps to 50 ns, for excitonic decay. Comparison of TA signals in the visible and near-infrared (NIR) spectral regions enables determination of the relative contributions of electron and hole dynamics to each decay component, and comparison of TA and TRPL reveals that each component represents a competition between radiative and nonradiative decay pathways. In total, these data suggest that the QD sample comprises at least three distinct populations that differ in both the radiative and nonradiative decay pathways available to the excitonic charge carriers, and provide evidence for multiple emissive excitonic states in which the hole is not in the valence band, but rather a relaxed or trapped state.

KEYWORDS: transient absorption · photoluminescence upconversion · time-correlated single photon counting · quantum dot · charge carrier trapping · radiative recombination

This paper describes a time-resolved, charge carrier-resolved map of decay from the first excitonic state of colloidal CdSe quantum dots (QDs). We constructed this map, which includes six distinguishable competitions between radiative and nonradiative decay pathways over the lifetime of the excitonic state in the sample, by performing a combination of transient absorption (TA) and time-resolved photoluminescence (TRPL) spectroscopy on a solution-phase ensemble of 5.0-nm QDs. Multiexponential dynamics of excitonic decay are common for colloidal QDs, due to heterogeneity in size, shape, degree of aggregation, and surface passivation and structure within a given QD sample.[1−3] This heterogeneity leads to a variety of decay processes available to band-edge excitons, where each observed time constant, τ, is an average excited state lifetime for a population of QDs with some set of available decay pathways ranging in time scale from hundreds of femtoseconds to microseconds.[1,4−9] Here, we show that the complementary techniques of TA and TRPL spectroscopies can yield enough information to build a comprehensive and physically meaningful picture of excitonic decay in CdSe QDs.

Our analysis has three characteristics that distinguish it from previous work on the excitonic dynamics of QDs: (i) We monitor both transient absorptions and emissions from the band-edge excitonic state of CdSe QDs over the time window of 100 fs to 500 ns, and show that these two types of experiments yield the same six time constants for excitonic decay. Previous studies have utilized PL upconversion,[5,10−17] ultrafast TA (fs-TA),[1,5−8,17−23] nanosecond TA (ns-TA),[24] and time-correlated single photon counting (TCSPC)[5,24,25] in various combinations, but here we use all four techniques on QDs with the same diameter and passivating ligands. (ii) We introduce a method for determining the relative contributions of electron dynamics and hole dynamics to each observed decay component by comparing signals in the visible and NIR regions of the TA spectra. Unlike previous studies,[8,17,21] including our own,[26] this method quantitatively partitions each component into electron and hole contributions, and does so utilizing samples with their native ligands; that is, it does not require treatment of the QDs with ligands intended to specifically perturb the dynamics of the electron or the hole. (iii) Using only TA and TRPL spectroscopy at room temperature, we provide evidence for multiple emissive excitonic states in which the hole is not in the valence band, but rather a relaxed or trapped state.

RESULTS AND DISCUSSION

Characterization of QD Samples. Figure 1 shows the ground state absorption spectrum of the CdSe QDs used in this study. The peak of the band-edge absorption feature is at 572 nm, and the average diameter of the QDs in the sample is 5.0 ± 0.6 nm as measured

* Address correspondence to e-weiss@northwestern.edu.

Received for review November 17, 2010 and accepted February 17, 2011.

Published online March 01, 2011
10.1021/nn2002689

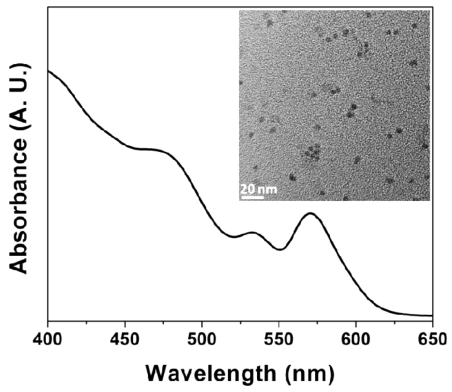

Figure 1. Ground-state absorption spectrum and representative TEM (inset) of 5.0-nm QDs; the peak of the band-edge absorption is at 572 nm.

by transmission electron microscopy (Figure 1, inset, see Supporting Information for size histogram). Dynamic light scattering measurements of the size distribution of a solution of the QDs in distilled $CHCl_3$ at the same concentration used for the TA measurements showed a single peak also centered at 5.0 nm (see Supporting Information); there is no evidence of aggregates in solution. Inductively coupled plasma atomic emission spectroscopy of the QDs indicates that, as previously reported[27,28] for samples prepared with commercially available technical grade TOPO (90%) as the coordinating solvent, these QDs are cadmium-enriched with a Cd/Se ratio of 2.3 ± 0.1.

TRPL and TA Yield Comparable Time Constants over a Dynamic Range of 6 Orders of Magnitude. *Dynamics Measured by TRPL.* Figure 2A shows the steady-state PL spectrum of the QDs in $CHCl_3$ excited at 534 nm. The peak of the PL is at 579 nm, and the fwhm of the PL peak is 22 nm; the QDs have a PL quantum yield of 5% in distilled $CHCl_3$. We monitored the time-dependence of the PL at 579 nm (marked with a dotted line in Figure 2A) using PL upconversion spectroscopy (instrument response function, IRF = 300 fs, Figure 2B) and time-correlated single photon counting (TCSPC, IRF = 280 ps, Figure 2B, inset). We used excitation energies higher than the bandgap (520 nm for the upconversion and 450 nm for the TCSPC) in order to avoid interference between the excitation source and the PL signal, which occurs at an energy that is only 0.02 eV less than the band-edge absorption. Excitation above the bandgap produces excitonic states with "hot" (above band-edge) holes, but the rise of the TRPL kinetic trace characteristic of intraband relaxation of hot carriers to the band-edge appears to be instrument-limited in our case.[5]

The TCSPC and PL upconversion kinetic traces (as well as the TA kinetic traces described below) were fit to a sum of exponential components, C_i eq 1,

$$C_i = A_i \exp\left[\frac{-t}{\tau_i}\right] \quad (1)$$

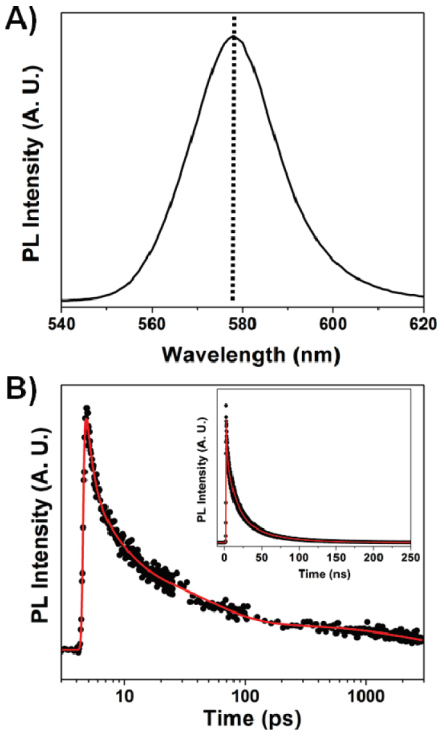

Figure 2. (A) Steady-state PL spectrum of the CdSe QDs; the dotted line indicates the wavelength at which we monitored the time-dependence of the PL using ultrafast PL upconversion (B) and TCSPC (B, inset).

TABLE 1. Time Constants (τ) for Decay Components C_1-C_6 Obtained from Multiexponential Fits of Features within Transient Absorption and TRPL Spectra

feature	τ_1 (ps)	τ_2 (ps)	τ_3 (ps)	τ_4 (ns)	τ_5 (ns)	τ_6 (ns)
TRPL peak (580 nm)[a]	0.73	4.5	48	1.4	13	45
VIS-TA GS bleach (572 nm)[b]		4.5	48	0.70	12	46
NIR-TA 900 nm		4.7	43	0.46	(9.2)[c]	
NIR-TA 1000 nm		3.2	35	0.28	(8.2)[c]	
NIR-TA 1100 nm		3.8	37	0.66	(13)[c]	
NIR-TA 1200 nm		2.9	30	0.43	(13)[c]	
NIR-TA 1300 nm		2.8	28	0.36	(13)[c]	
NIR-TA 1400 nm		2.5	26	0.39	(15)[c]	

[a] Values of τ_4, τ_5, and τ_6 are measured by TCSPC. Values of τ_1, τ_2, and τ_3 are measured by PL upconversion. [b] Values of τ_5 and τ_6 are measured by ns-TA. Values of τ_2, τ_3, and τ_4 are measured by fs-TA. [c] Values of τ_5 in parentheses are necessary components to achieve a good fit of the kinetic trace, but are not necessarily measured accurately by the fs-TA experiment because they lie outside the experiment's time window.

where each C_i has an associated time constant, τ_i, and amplitude, A_i. To compare amplitudes among different wavelengths, we normalize the amplitudes for each kinetic trace such that $\sum_i A_i = 1$. The kinetic trace from the PL upconversion experiment fit to a sum of four exponentials with time constants of 730 fs, 4.5 ps, 48 ps (τ_1, τ_2, and τ_3 in Table 1), and 3 ns. The kinetic trace from the TCSPC experiment fit to a sum of three exponentials with time constants of 1.4, 13, and 45 ns (τ_4, τ_5, and τ_6 in Table 1). We interpret the 3-ns time constant in the upconversion trace to be a weighted

average of τ_4 and τ_5 measured with TCSPC, which is more accurate than upconversion on the nanosecond time scale because its time window is 280 ps to 500 ns, whereas the time window for upconversion is 300 fs to 3000 ps. The time constants in Table 1 agree with excitonic lifetimes in the ranges of 2−5 ps[10−16,20,21,29] (τ_2) and 30−50 ps,[8,10,11,13,17,21,29] (τ_3) measured with both fs-TA and PL upconversion by several groups, and with average lifetimes of ~20 ns (τ_4, τ_5, and τ_6) measured with TCSPC[5,21,30,31] for similarly sized CdSe QDs in solution.

Since the PL quantum yield of the QD sample is less than 100%, we are not just observing the natural radiative lifetimes of several populations of QDs; rather, each time constant, τ, in the time-resolved decay of PL intensity is an average lifetime that results from a competition between at least one radiative rate of decay, k_r, and at least one nonradiative rate of decay, k_{nr}, eq 2.

$$\tau = \frac{1}{k_r + k_{nr}} \quad (2)$$

Dynamics Measured by TA. In many cases, a fit to a sum of four exponentials (as we use for the femtosecond data) is difficult to distinguish from a fit with a continuous distribution of exponentials. We therefore rigorously compared fits of all of our datasets (TRPL and TA) with sums of exponentials to fits including stretched exponentials and fits to the Tachiya model, which describes the decay of the excited states *via* Poisson-distributed pathways (see the Supporting Information). Our major conclusions are: (i) use of the distributed functions (stretched and Poisson-derived exponentials) did not decrease the number of fitting parameters required to obtain adequate fits of the data (as measured by uniform scattering of residuals across a zero line); (ii) stretched exponentials (and combinations of stretched exponentials with single exponentials) fit only select data sets; and (iii) the Poisson-derived fits, which are appealing for our system because they, in principle, separate radiative and nonradiative pathways, are completely equivalent to the multiexponential fits in that their fitting parameters are just linear combinations of the set of fitting parameters obtained from the multiexponential fits (we demonstrate the transformation between the two sets of functions in the Supporting Information). Furthermore, use of the Poisson functions in the analysis of electron and hole contributions to each decay process yields a quantitatively similar answer to that we get using the multiexponential fits (as described in the next section). We are therefore confident that, although our four-exponential fit function is not a unique fit of the data, it is a member of a set of functions that fit the data adequately with the fewest fitting parameters, and that each member of this set of functions leads to the same mechanistic interpretation of the data.

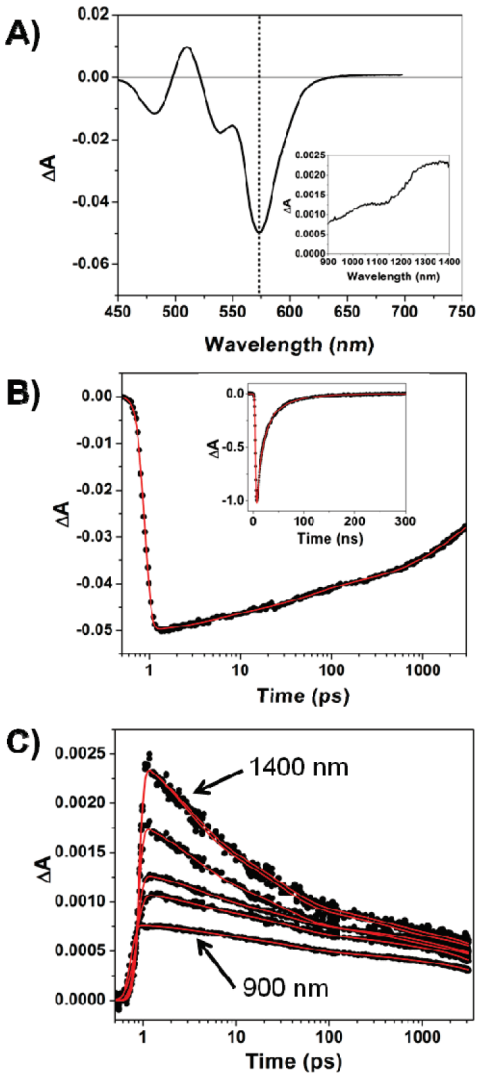

Figure 3. (A) Transient absorption spectra of QDs in $CHCl_3$ obtained by exciting to the first excitonic state and probing in the visible and NIR (inset). Both spectra are shown at the peak of the instrument-limited rise in signal. (B) Kinetic trace of the recovery of the ground state bleach at 572 nm (indicated by the dotted line in A) on the femtosecond and nanosecond (inset) time scales. The fs-TA kinetic trace is fit to a sum of four exponential functions, and the ns-TA trace is fit to a sum of two exponential functions. (C) Kinetic traces of the decays of excited state absorptions at 100-nm intervals from 900 to 1400 nm. These kinetic traces are fit to a sum of four exponential functions.

Figure 3A shows TA spectra of the QDs in $CHCl_3$ in the visible and NIR (inset) regions, obtained by probing these regions following excitation of the QDs at 572 nm, the peak of the band-edge absorption. The TA spectra shown in Figure 3A are described in detail elsewhere;[7,26] the major feature in the visible region (the peak of which is marked by the dotted line) is the bleach of the ground state (GS) band-edge absorption of the QDs induced by photoexcitation by the pump beam. Because of the large near-degeneracy of valence band-edge states compared to conduction band-edge states in CdSe QDs, the recovery of the

GS bleach exclusively reflects the dynamics of depopulation of electrons from the conduction band-edge states.[6,8,17]

The fs-TA kinetic trace at the GS bleach (IRF = 200 fs, Figure 3B) fits to a sum of four exponentials, with time constants of 4.5 ps, 48 ps, and 0.70 ns (listed as τ_2, τ_3, and τ_4 in row 2 of Table 1) and 11 ns. The ns-TA kinetic trace at the GS bleach (IRF = 7 ns, Figure 3B, inset) fits to a sum of two exponentials with time constants of 12 and 46 ns (τ_5 and τ_6 in row 2 of Table 1). The values of τ_5 measured by ns-TA and fs-TA are within 8% of each other, and the values of τ_5 and τ_6 measured by ns-TA are within 8% of the two longest time constants measured by TCSPC. Furthermore, the values of τ_2 and τ_3 measured with fs-TA at the GS bleach are within 2% of the values measured by PL upconversion; in the fits of both the TA and PL data, these two time constants were insensitive to variation of the longer time constants. In contrast, τ_4 (~1 ns) was the least robust time constant in all fits; it was sensitive to the time constants and amplitudes of both faster and slower components. We believe this sensitivity accounts for the discrepancy between the values of τ_4 measured by TA and PL (which differ by a factor of 2).

Figure 3A, inset, shows the NIR-TA spectrum from 900 to 1400 nm. This region contains overlapping spectra of transitions of the electron and hole in band-edge states to higher-energy excited states; decay of the NIR features therefore corresponds to depopulation of these band-edge states by the excitonic electrons and holes. We[26] and others[17] have shown previously that hole transitions contribute primarily to the low-energy side of the NIR spectrum, and the high-energy side of the spectrum is due primarily to electron transitions. We fit a series of kinetic traces from 900−1400 nm to a sum of four exponentials (IRF = 200 fs, Figure 3C). We found that τ_2, τ_3, and τ_4 vary as a function of wavelength across the NIR region (rows 3−8 in Table 1): the time constants measured at the high-energy end of the NIR (*i.e.,* 900 nm) are most similar to those measured at the GS bleach, and, in general, the time constants decrease on going from 900 to 1400 nm (although τ_4 oscillates somewhat). The decrease in time constants is concurrent with an increase in the amplitude of C_2, the fastest observed component in the TA decay (see the Supporting Information for a table of amplitudes from the single-wavelength fits in the visible and NIR).

We believe that the decrease in the observed values of τ_2, τ_3, and τ_4, and the increase in the amplitude of C_2 on going from 900 to 1400 nm are due to the contribution of C_1, the subpicosecond component that we resolve in the TRPL kinetic trace, to the low-energy region of the spectrum. We cannot resolve C_1 from C_2 in the TA kinetic traces in either the NIR or visible regions; that is, the quality of the fit of these kinetic traces does not improve significantly upon increasing

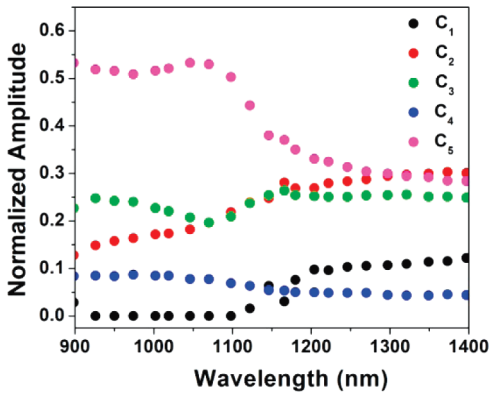

Figure 4. Normalized amplitudes of C_1−C_5 from a global regression analysis of kinetic traces at 25 nm intervals from 900 to 1400 nm, in which τ_1 was fixed to 0.73 ps and τ_2−τ_5 were fixed to the values of τ_2−τ_5 from the fit of the recovery of the GS bleach (Table 1).

the fit function from four to five exponentials, as judged by negligible changes in the scattering of residuals across a zero line and in the value of χ^2 for the fit. The observation that the values of τ_2 and τ_3 from the kinetic trace of the GS bleach match the values of τ_2 and τ_3 from the PL indicates that C_1 does not contribute significantly to the recovery of the GS bleach. To confirm that the decrease in τ_2, τ_3, and τ_4 across the NIR spectrum is due to the contribution from C_1, we performed a global fit of 21 kinetic traces across the NIR to a sum of five exponentials, in which τ_1 was fixed to 0.73 ps (the time constant we obtained with TRPL), and τ_2−τ_5 were fixed to the values of τ_2−τ_5 obtained from fitting the recovery of the GS bleach (row 2, Table 1); in other words, we manually deconvolved C_1 and C_2 in the NIR kinetics. We found from this fit that the normalized amplitude of C_1 is zero for wavelengths from 925 to 1100 nm (the electron side of the spectrum) and increases on going from 1100 to 1400 nm (the hole side of the spectrum), Figure 4. We conclude from the observations that C_1 does not contribute to the recovery of the GS bleach, and that C_1 only appears to contribute to the region of the NIR spectrum that contains signal from hole-mediated decay processes, that C_1 is an ultrafast hole relaxation process that out-competes any available charge recombination pathways. This subpicosecond component—which has been observed previously as a discrepancy between dynamics at ~1400 nm and dynamics at the GS bleach,[21,29] but not identified—cannot be due to relaxation of an energetically hot hole to the edge of the valence band because intraband relaxation would manifest as a rise in the PL upconversion trace rather than a decay.[5]

The one-to-one correspondence between dynamics measured by TA and those measured by TRPL is an important result. This result indicates that each excitonic lifetime, τ, we observe in TA is a lifetime defined by eq 2; each lifetime originates from a state

that is potentially emissive, but is competing with a nonradiative quenching process. The TA data alone could not have revealed this result because TA only indicates that charge carriers are depopulating their band-edge states; it does not tell us that the states from which these particles decay are potentially radiative states. In formulating our mechanism for excitonic decay, we assume the simplest case: that only one radiative rate and one nonradiative rate compete to yield each observed excitonic lifetime, although we acknowledge that each of these rates could be an effective rate constant that is the sum of rates for several processes.

A Comparison of VIS- and NIR-TA Spectra Reveals the Contributions of Each Charge Carrier to Each Component of Excitonic Decay. Comparison of PL and TA data has revealed that each of the six decay components that we observe reflects a competition within the ensemble of QDs between a radiative recombination, which, by definition, has equal contributions from electrons and holes, and a nonradiative decay. Nonradiative decay processes in QDs can involve only the electron (electron trapping), only the hole (hole trapping), or both (Auger recombination, for example).[32] The following analysis of the visible and NIR TA spectra allows us to determine the relative contributions of electron and hole dynamics to each decay component.

Equation 3 is an expression for $\eta_{n,e}$, the fraction of the total normalized amplitude of a given component C_n that is accounted for by electron decay; $1 - \eta_{n,e}$ is the fraction of the amplitude of C_n accounted for by hole decay.

$$\eta_{n,\mathrm{e}} = \frac{\chi_{n,\mathrm{e}}}{\chi_{n,\mathrm{e}} + \chi_{n,\mathrm{h}}} \tag{3}$$

In eq 2, $\chi_{n,e}$ and $\chi_{n,h}$ denote the fraction of the total population of electrons and holes, respectively, in band-edge states that decay *via* C_n. To determine $\eta_{n,e}$, we need to find $\chi_{n,e}$ and $\chi_{n,h}$. We can calculate $\chi_{n,e}$ and $\chi_{n,h}$ by comparing the normalized amplitudes of each component at two wavelengths in the TA spectrum: one wavelength at which 100% of the spectral amplitude results from electron transitions, and one wavelength at which 50% of the spectral amplitude originates from hole transitions and 50% originates from electron transitions. We could do the calculation with any two wavelengths for which we know the relative spectral amplitudes of electron and hole, but it is simplest with this combination of wavelengths. The wavelength at which 100% of the amplitude is due to electron transitions is the GS bleach; we will call this wavelength λ_{VIS}. The Supporting Information describes in detail how we determined the wavelength in the NIR at which the electron and hole contribute equally to the spectral amplitude; it is 1170 nm for the 5.0-nm CdSe QDs used in this study, and we denote it λ_{NIR}.

TABLE 2. Normalized Amplitudes (A) and Ratios of Amplitudes (A_{VIS}/A_{NIR}) for Decay Components Obtained from Transient Absorption Measurements

feature	A_1	A_2	A_3	A_4	$A_5 + A_6$
VIS-TA GS bleach (λ_{VIS} = 572 nm)	0.0	0.061	0.12	0.092	0.73
NIR-TA absorption (λ_{NIR} = 1170 nm)	0.033	0.28	0.26	0.055	0.37
A_{VIS}/A_{NIR}[a]	0.0	0.22	0.46	1.7	2.0
% electron/% hole	0/100	11/89	23/77	85/15	100/0

[a] A_{VIS} is the normalized amplitude of each component at the wavelength of the peak of the GS bleach; A_{NIR} is the normalized amplitude of each component at the wavelength in the NIR where electron and hole contribute equally to the spectral amplitude, 1170 nm.

We first find $\chi_{n,e}$, the fraction of the total population of electrons in conduction band-edge states that decay *via* C_n, by fitting the kinetic trace at λ_{VIS} (= 572 nm). Since the kinetic trace at λ_{VIS} only reflects electron dynamics, $\chi_{n,e}$ is equivalent to the normalized amplitude of C_n at λ_{VIS}: $\chi_{n,e} = A_{n,VIS}$. Next, to find $\chi_{n,h}$, we examine the kinetic trace at λ_{NIR} (= 1170 nm). The normalized amplitude of C_n at λ_{NIR}, $A_{n,NIR}$, has contributions from electron and hole dynamics, eq 4.

$$A_{n,\mathrm{NIR}} = A_{n,\mathrm{NIR,e}} + A_{n,\mathrm{NIR,h}} \tag{4}$$

Since the electron and the hole contribute equally to the spectral amplitude at λ_{NIR}, the amplitude of the electron-mediated portion of the decay, $A_{n,NIR,e}$, and the amplitude of the hole-mediated portion of the decay, $A_{n,NIR,h}$, are given by eq 5.

$$\begin{aligned} A_{n,\mathrm{NIR,e}} &= \chi_{n,\mathrm{e}} 0.5 \\ A_{n,\mathrm{NIR,h}} &= \chi_{n,\mathrm{h}} 0.5 \end{aligned} \tag{5}$$

Combining eqs 4 and 5, substituting $A_{n,VIS}$ for $\chi_{n,e}$, and solving for for $\chi_{n,h}$ yields eq 6:

$$\chi_{n,\mathrm{h}} = 2A_{n,\mathrm{NIR}} - A_{n,\mathrm{VIS}} \tag{6}$$

Finally, substituting eq 6 for $\chi_{n,h}$ and $A_{n,VIS}$ for $\chi_{n,e}$ in eq 3 yields eq 7:

$$\eta_{n,\mathrm{e}} = 0.5\frac{A_{n,\mathrm{VIS}}}{A_{n,\mathrm{NIR}}} \tag{7}$$

which expresses $\eta_{n,e}$, the fractional contribution of electron dynamics to C_n, in terms of the experimentally observable quantities $A_{n,VIS}$ and $A_{n,NIR}$. Equation 7 quantitatively formulates the "electron character" (and, therefore also the "hole character") of a given component, C_n.

Three simple examples of the application of this amplitude analysis are (i) if $A_{n,VIS}/A_{n,NIR} = 2$ for a particular component, then $\eta_{n,e} = 1$ and 100% of the component is due to electron decay; (ii) if $A_{n,VIS}/A_{n,NIR} = 0$, then $\eta_{n,e} = 0$, and 100% of the component is due to hole decay; (iii) if $A_{n,VIS}/A_{n,NIR} = 1$, then $\eta_{n,e} = 0.5$, and the decay component is due to a process that has equal contributions from electron and hole transitions.

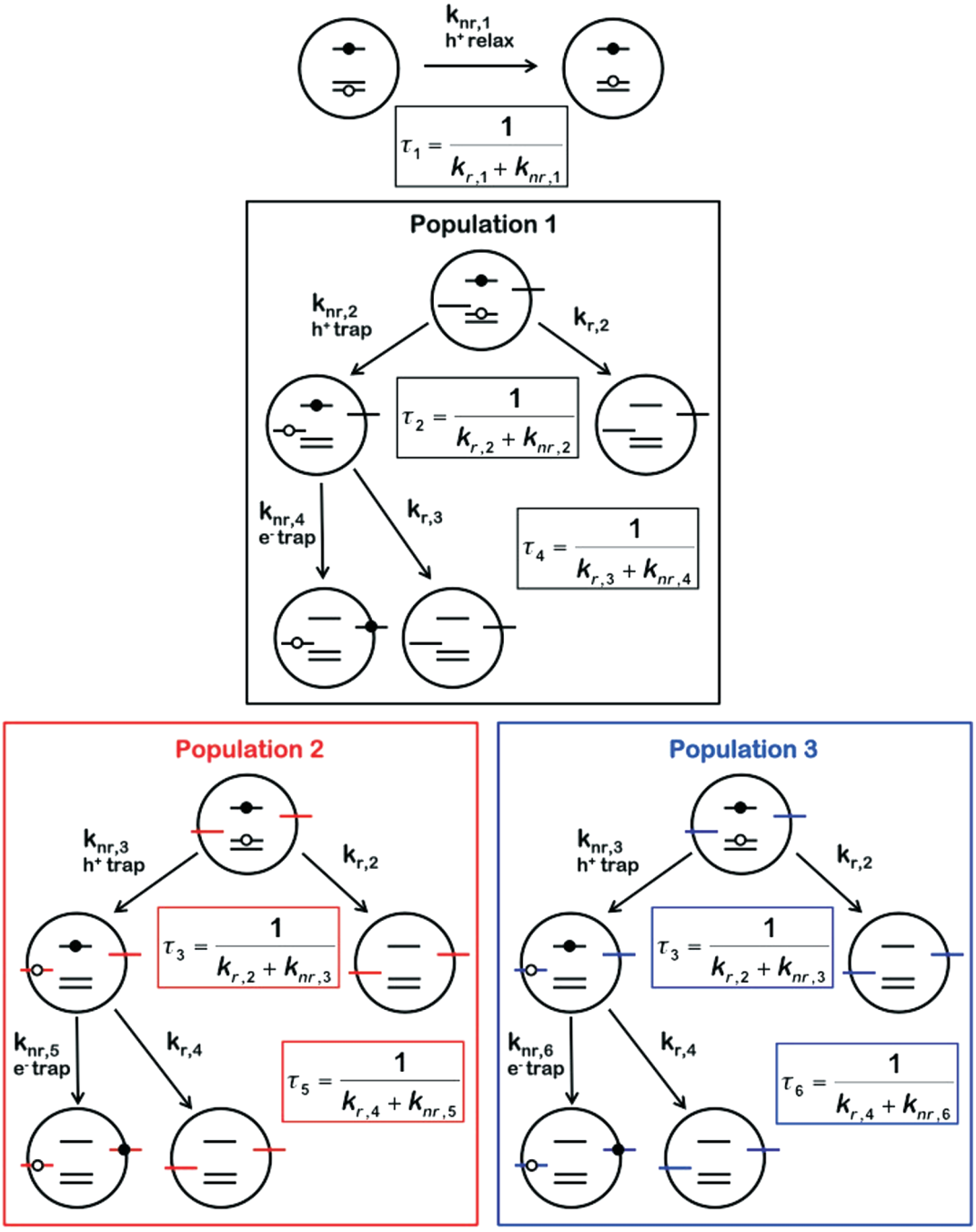

Figure 5. Illustration of the decay pathways that are available upon photoexcitation to the different populations of QDs present in our sample.

We do not know the relative oscillator strengths of the intraband transitions of electrons and holes measured by NIR TA,[33] so we cannot calculate the relative populations of electrons and holes that participate in each decay component from their relative amplitudes. We can safely assume, however, that the oscillator strengths of the two charge carriers are similar because the total spectral amplitude in the NIR region, which includes signals from both electron and hole transitions created from a single pump pulse, does not vary by more than a factor of 3 on going from 900 nm, where the spectral amplitude originates almost exclusively from the electron, to 1400 nm, where the spectral amplitude originates from both the electron and the hole.

Assignment of Charge Carrier Contributions to Each Decay Component Based on the Amplitude Analysis. Table 2 lists $A_{n,VIS}/A_{n,NIR}$, where λ_{VIS} = 572 nm and λ_{NIR} = 1170 nm, for the components observed in the TA experiments. We use the normalized amplitudes A_1-A_5 from the five-exponential global fit of the fs-TA NIR kinetics (where τ_1 was fixed to 730 fs) in this analysis in order to separate the contributions of C_1 and C_2. In addition,

we did not measure C_5 and C_6 in the NIR (because we do not have a NIR probe for ns-TA), but we do know their combined amplitude in the NIR—it is simply the amplitude of C_5 in the global fit of the fs-TA kinetic trace. We therefore perform the amplitude analysis using their combined amplitude, $A_5 + A_6$.

Figure 5 is the map of excitonic decay that we derive from the assignments based on the amplitude analysis. For C_1, $A_{VIS}/A_{NIR} \approx 0$, so, by eq 7, 100% of this component is due to decay of the hole. We believe C_1 is a competition between radiative recombination from the initially prepared exciton (with rate constant $k_{r,1}$) and nonradiative, hole-mediated relaxation of this exciton (with rate constant $k_{nr,1}$), Figure 5, top. The fact that there is no apparent contribution from the radiative recombination (which would appear as contribution from the electron) to this component indicates that nonradiative hole relaxation completely dominates over radiative recombination, $k_{nr,1} \gg k_{r,1}$, so τ_1 is effectively the time constant for hole relaxation. Since C_1 is such a prominent feature in the TRPL decay (it accounts for ~40% of the total amplitude of the decay), we assume that this initial relaxation process occurs on all of the QDs in the sample, and that the "relaxed" exciton is the starting point for all subsequent dynamics.

For C_2, $A_{VIS}/A_{NIR} = 0.22$, so, by eq 7, 89% of this component is due to decay of the hole and 11% is due to decay of the electron. The presence of a minor contribution of electron dynamics to C_2 indicates that, as suggested previously,[8,10,11,13,15−17,20,26] this component is a competition between radiative recombination from the relaxed excitonic state (with rate constant $k_{r,2}$) and a hole-trapping process from the relaxed excitonic state into shallow defect states intrinsic to the QD lattice (with rate constant $k_{nr,2}$), where hole-trapping dominates: $k_{nr,2} > k_{r,2}$ (Figure 5, Population 1).

For C_3, $A_{VIS}/A_{NIR} = 0.46$, so C_3 is 77% hole and 23% electron; the majority contribution from the hole indicates that this component must also be due to a competition between radiative recombination and hole trapping (Figure 5, Populations 2 and 3). The bigger contribution of the electron to this component than to C_2 indicates that radiative recombination is more competitive with hole trapping within C_3 than within C_2. A simple explanation for this result is that the hole-trapping process for QDs that decay *via* C_3 is slower than the hole-trapping process for QDs that decay *via* C_2 ($k_{nr,3} < k_{nr,2}$), so recombination, $k_{r,2}$, is more competitive with $k_{nr,3}$ than with $k_{nr,2}$, and the overall observed excitonic lifetime is longer: $\tau_3 > \tau_2$. In this case, we observe both τ_2 and τ_3 lifetimes because there are two populations (Population 1 and Populations 2/3 in Figure 5) of QDs in the sample differentiated by the distribution of available hole traps.

For C_4, $A_{VIS}/A_{NIR} = 1.7$, so C_4 is 15% hole and 85% electron. The majority contribution from the electron indicates that C_4 is a competition between electron-trapping and charge recombination (Figure 5, Population 1), where the electron-trapping process (with a rate constant $k_{nr,4}$) dominates over the radiative process, with rate constant $k_{r,3}$. The radiative process that contributes to this component must be slower than 1 ns in order for us to observe an overall lifetime of ~1 ns, so it must be a different radiative process than that which contributes to C_2 and C_3, $k_{r,2}$, which effectively competes with hole-trapping to produce an average lifetime of ~50 ps. We suspect that the $k_{r,3}$ process is the recombination of a conduction band-edge electron with a trapped hole formed during the C_2 process (Population 1).

For the combination of C_5 and C_6, $A_{VIS}/A_{NIR} = 2.0$, so both C_5 and C_6 correspond to decay processes that are due exclusively to electron dynamics. We still observe PL from the sample on the 10−50-ns time scale (Figure 2B, inset) even though hole dynamics do not contribute to decay components (C_5 and C_6) observed in the TA on this time scale. The PL must therefore originate from excitonic states in which the hole is trapped, perhaps in a surface state that is decoupled from the valence band, and no longer contributes to spectral amplitude in the NIR TA. We can therefore assign the decay processes corresponding to C_5 and C_6 to competition between nonradiative electron-trapping processes and radiative recombination of band-edge electrons with trapped holes. The observation of two distinct components of this type, C_5 and C_6, probably indicates that there are two populations of QDs with the same radiative rate constant, $k_{r,4}$, but different distributions of available electron traps, and therefore different rates of nonradiative decay, $k_{nr,5}$ (Population 2) and $k_{nr,6}$ (Population 3).

The observation that recombination of band-edge electrons and trapped holes is observable by PL implies that the hole-trapped excitons are emissive, and furthermore, that these excitons have a PL spectrum that overlaps that of the band-edge state. The presence of emissive states in which the hole is removed from the valence band-edge, but with energies near that of the bandgap (*i.e.*, not deep-trap emission) was reported previously.[1] The observed decays of PL on the time scales of hole trapping, (3−50 ps) are due to changes in yield of emission from the relaxed state formed by $k_{nr,1}$ to the trapped hole states formed by $k_{nr,2}$ and $k_{nr,3}$. Our mechanism tells us that the hole-trapping processes do not completely quench the PL on their own; the final decay of potentially emissive excitonic states is accomplished by a combination of electron trapping and radiative recombination.

We repeated this amplitude analysis on another batch of CdSe QDs that are slightly larger, $\lambda_{abs} = 577$ nm, see Supporting Information, and we obtained similar charge carrier assignments for each of the measured components for both batches of QDs.

CONCLUSIONS

Our combined TA and TRPL data sets indicate that there are three populations of QDs present in the sample; these populations differ by the types of decay pathways available to the excitonic charge carriers, as outlined in Figure 5. The map that we propose for decay of the first excitonic state of CdSe QDs is not the only possible picture, but it is the simplest physically reasonable picture suggested by the fits of our data. We show (in the Supporting Information) that the multiexponential functions we use to model our kinetic traces are the simplest (with respect to number of fitting parameters) functions that adequately fit the data, and that this minimum number of fitting parameters is not reduced by fitting the data with a continuously distributed exponential function (such as a stretched exponential). The TA and TRPL techniques, as we have applied them here, do not give us information about the structural and/or chemical origins of the states present in our mechanism, although the consistent appearance of the 2−5-ps and 30−70-ps decay components in the literature—for CdSe and CdS QDs with multiple types of surface passivation, and in multiple solvents[8,10−17,20,21,29]—implies that the processes producing these lifetimes involve states, as others have suggested, that are "intrinsic" to the QD core lattice. Our conclusion that the excitonic states formed by nonradiative trapping of the hole on these time scales still have enough electron−hole coupling to be emissive is then not surprising.

The evolution of the excitonic state in colloidal QDs is system-specific, even for a given size and material of QD, but several general lessons emerge from this work that will facilitate interpretation of the dynamics of a range of solution-phase (and possibly solid phase) QD ensembles: (i) Transient absorption and time-resolved PL yield consistent results and provide complementary information about the evolution of band-edge excitons, but only if both are used to examine the same time window (subpicosecond to hundreds of nanoseconds). Probing different time windows with each technique, or probing only a portion of the total lifetime of the exciton can be misleading. (ii) Comparison of the TA spectra in the visible and NIR regions yields quantitative information about the relative contributions of electron and hole-mediated processes to each observed decay component. (iii) There are several potentially emissive excitonic states in which the hole is not in its initial delocalized core state. Radiative recombination from these relaxed or trapped hole states has a different rate than recombination from the initial core state. This result implies that, in mapping excitonic decay, there are several values of k_r to consider. Multiexponential behavior is not just caused by variation in available nonradiative pathways, but also by variation in available radiative pathways throughout the ensemble. It is possible that a given observed k_r results from an equilibrium between an emissive excitonic state and a state in which one of the carriers is trapped, in which case variation in k_r originates from variation in k_{nr}. (iv) In the types of CdSe QDs we studied, which are Cd-enriched and therefore have little to no Se on the surface, it appears that trapping of the hole does not directly quench the PL of the QD, but rather increases the radiative lifetime such that nonradiative electron-trapping processes on the 1−100 ns time scale are competitive with PL.

The results that we derive in this work for QDs with their native ligands will serve as a starting point for analyzing the mechanisms by which treatment of the QDs with other common ligands, such as thiols, anilines, alkylamines, and acids either quenches or enhances the PL quantum yield of the sample.[34−39]

EXPERIMENTAL METHODS

Synthesis and Purification of QDs. We synthesized colloidal CdSe QDs using the organometallic precursor-based procedure of Qu, *et al.*[40] with minor modifications (see Supporting Information). We arrested the growth of the QDs after injection of the Se precursor, TOPSe, which was prepared and stored in a glovebox, by quickly cooling the reaction with 10 mL of hexanes. The solution sat for 12 h in the dark, during which time a white precipitate (excess cadmium stearate, TOPO, and HDA) formed. Centrifugation of this suspension at 3500 rpm for 5 min separated a white pellet of excess ligand, which we discarded, from a red supernate that contained the QDs. The addition of methanol to the supernate (1:1 by volume) and further centrifugation produced a red pellet of QDs and a colorless supernate containing HDA and TOPO. We discarded the supernate, dried the QD pellet with a stream of nitrogen, and stored it in the dark under a nitrogen atmosphere until use.

ICP-AES. We prepared a sample and calibration standards for ICP-AES as detailed in the Supporting Information. We acquired the data on a Varian Vista-MPX instrument and analyzed it using Varian's ICP-expert II software. We calculated the elemental concentrations using the calibrated intensities of the Cd atomic emission peak at 214.439 nm and the Se atomic emission peak at 196.026 nm. The value and error we report for the elemental ratio Cd/Se are the average and standard deviation, respectively, of three different measurements of the same sample.

Steady-State Photoluminescence. To prepare samples for PL measurements, we diluted the QD pellet in distilled $CHCl_3$ to an optical density (O.D.) of 0.08 in a 1 cm quartz cuvette at the maximum of the band-edge absorption of the QDs, $\lambda = 572$ nm. We collected the emission spectra on a Fluorolog-3 spectrofluorimeter (Horiba JobinYvon Spex) with an excitation wavelength of $\lambda_{exc} = 534$ nm over a range of 540−700 nm. We chose $\lambda_{exc} = 534$ nm to minimize the contribution of scattered excitation light in the emission spectrum. The emission and excitation slit widths were set to pass an effective bandwidth of 2 nm. The PL quantum yield of the solution of QDs was determined relative to an optically matched sample of Rhodamine 101 as detailed in the Supporting Information.

Ultrafast Transient Absorption. The transient absorption setup, with visible and NIR continuum probes, is described in detail elsewhere,[26] and in the Supporting Information. The sample was prepared with an absorbance of 0.15 at the maximum of the band-edge absorption feature in a 2 mm cuvette, to ensure that both pump and probe light interact with the CdSe QDs

uniformly across the sample thickness. The pump light was depolarized to prevent unintentional photoselection so that measurements reflect only population dynamics. Incident pump fluence was adjusted to produce an expected excited state population of 30% (see Supporting Information for the calculation). The solution was stirred with a magnetic stir bar to minimize local heating.

Nanosecond Transient Absorption. Samples for nanosecond transient absorption spectroscopy[41] were prepared by dispersing QDs in distilled $CHCl_3$ to an OD of 0.8 at the band-edge absorption feature and placed in a 1 cm path length quartz cuvette. The samples were excited with 7 ns, 1.5 mJ, 560 nm laser pulses using the frequency-tripled output of a Continuum Precision II 8000 Nd:YAG laser pumping a Continuum Panther optical parametric oscillator (OPO). The excitation pulse was focused to a 8 mm diameter spot and matched to the diameter of the probe pulse generated using a xenon flashlamp (EG&G Electro-Optics FX-200). Kinetic traces were observed from 450 to 700 nm every 5 nm using a monochromator and photomultiplier tube with high voltage applied to only four dynodes (Hamamatsu R928), and recorded with a LeCroy Wavesurfer 42Xs oscilloscope interfaced to a customized Labview program (Labview v. 8.5.2). The total instrument response time is 7 ns and is determined primarily by the laser pulse duration. We monitored the bleach of the ground state at 555 nm, a higher energy than the peak of the ground-state (GS) bleach feature (572 nm), in order to minimize the amount of pump scatter and photoluminescence from the QD captured by the detector.

Time-Correlated Single Photon Counting. A 450-nm diode laser (PicoQuant model no. LDH-P-C-450B) operating at a 2 MHz rep rate was used to excite a sample of QDs dispersed to an O.D. of 0.1 at the band-edge maximum in distilled $CHCl_3$ as it was stirred in a 1-cm four-sided quartz cuvette. Photons emitted from the sample were focused into a fiber optic cable located perpendicular to the excitation source. The output of the fiber was passed through a double monochromator (Spectral Products CM112) set to 579 nm (the peak of the steady-state emission). A second fiber optic guided the output of the monochromator onto the photocathode of a photomultiplier tube (PMT, Hamamatsu H5783−20). A timer−counter−analyzer with 50 ps bin size resolution (Pendulum CNT91) was used to measure the difference in time between the start signal from the PMT and the stop signal from the nuclear instrumentation module (NIM) synchronization output of the laser controller. The laser fluence was adjusted so that the ratio of the number of counted signals from the PMT to the number of laser pulses in the same time period was less than 0.01 to ensure that counting obeyed Poisson statistics. The instrument response time was 280 ps as measured by the full-width-at-half-maximum (fwhm) of the counting histogram of laser light from an elastic scattering sample.

Photoluminescence Upconversion. Part of the 800 nm, 150 kHz output of a Coherent RegA 100−250 kHz system was sent into an optical parametric amplifier (OPA) where the 520 nm pump pulse was generated, while the other portion was used as the gate pulse. The pump pulse was sent through a prism pair to compress the pulse to ~50 fs, and afterward was sent along with the gate into an Ultrafast Systems Halcyone setup. The gate was directed to a retroreflector on a delay stage; the pump was focused onto a 2 mm cuvette containing QDs dispersed to an OD of 0.15 at the band-edge in $CHCl_3$. The sample was stirred with a magnetic stirrer to reduce sample degradation and heating effects. After passing through a low-pass filter, photoluminescence generated in the sample was focused together with the gate pulse onto a β-BaB_2O_4 (BBO) crystal to create a sum-frequency generation (SFG) signal, which was then focused into a monochromator and into a PMT. The time-response was 300 fs, as determined by the fwhm of an upconverted Raman peak of toluene. We varied the time delay between the pump and gate pulses by moving the retroreflector on the delay stage in order to obtain a kinetic trace of the SFG signal.

Acknowledgment. K. Knowles is funded by the MRSEC program of the National Science Foundation (DMR-0520513). We made use of public facilities within the NUANCE Center at Northwestern University. The NUANCE Center is supported by NSF-NSEC, NSF-MRSEC, Keck Foundation, the State of Illinois, nd Northwestern University. E. McArthur would like to thank the Dreyfus Foundation Postdoctoral Program in Environmental Chemistry for a fellowship. The authors thank Michael Vagnini and Michael Wasielewski for use of and assistance with their nanosecond transient absorption setup, Michael Mara and Lin Chen for use of and assistance with their PL upconversion system, and David Walker and Bartosz Grzybowski for use of and assistance with the dynamic light scattering setup.

Supporting Information Available: Experimental details, histogram of QD diameters measured by TEM and dynamic light scattering, residuals plots for the multiexponential fits of TA and TRPL dynamics and comparison with distributed fits, normalized amplitudes of C_2-C_6 obtained from four-exponential fits of TA kinetics at individual wavelengths in the NIR, determination of the "50/50" wavelength, fs-TA data from QDs with λ_{abs} = 577 nm, Tables S1−S12 and Figures S1−S7. This material is available free of charge *via* the Internet at http://pubs.acs.org.

REFERENCES AND NOTES

1. Bawendi, M. G.; Wilson, W. L.; Rothberg, L.; Carroll, P. J.; Jedju, T. M.; Steigerwald, M. L.; Brus, L. E. Electronic Structure and Photoexcited-Carrier Dynamics in Nanometer-Size CdSe Clusters. *Phys. Rev. Lett.* **1990,** *65*, 1623–1626.
2. Alivisatos, A. P.; Harris, T. D.; Carroll, P. J.; Steigerwald, M. L.; Brus, L. E. Electron-Vibration Coupling in Semiconductor Clusters Studied by Resonance Raman Spectroscopy. *J. Chem. Phys.* **1989,** *90*, 3463–3468.
3. Norris, D. J.; Nirmal, M.; Murray, C. B.; Sacra, A.; Bawendi, M. G. Size-Dependent Optical Spectroscopy of II−VI Semiconductor Nanocrystallites (Quantum Dots). *Z. Phys. D* **1993,** *26*, 355–357.
4. Mittleman, D. M.; Schoenlein, R. W.; Shiang, J. J.; Colvin, V. L.; Alivisatos, A. P.; Shank, C. V. Quantum Size Dependence of Femtosecond Electronic Dephasing and Vibrational Dynamics in CdSe Nanocrystals. *Phys. Rev. B* **1994,** *49*, 14435–14447.
5. Wang, H.; de Mello Donega, C.; Meijerink, A.; Glasbeek, M. Ultrafast Exciton Dynamics in CdSe Quantum Dots Studied from Bleaching Recovery and Fluorescence Transients. *J. Phys. Chem. B* **2006,** *110*, 733–737.
6. Sewall, S. L.; Cooney, R. R.; Anderson, K. E. H.; Dias, E. A.; Kambhampati, P. State-to-State Exciton Dynamics in Semiconductor Quantum Dots. *Phys. Rev. B* **2006,** *74*, 1–8.
7. Kambhampati, P. Unraveling the Structure and Dynamics of Excitons in Semiconductor Quantum Dots. *Acc. Chem. Res.* **2011,** *44*, 1–13.
8. Klimov, V. I.; McBranch, D. W.; Leatherdale, C. A.; Bawendi, M. G. Electron and Hole Relaxation Pathways in Semiconductor Quantum Dots. *Phys. Rev. B* **1999,** *60*, 13740–13749.
9. Jones, M.; Scholes, G. D. On the Use of Time-Resolved Photoluminescence as a Probe of Nanocrystal Photoexcitation Dynamics. *J. Mater. Chem.* **2010,** *20*, 3533–3538.
10. Garrett, M. D.; Dukes, A. D., III; McBride, J. R.; Smith, N. J.; Pennycook, S. J.; Rosenthal, S. J. Band Edge Recombination in CdSe, CdS and CdS_xSe_{1-x} Alloy Nanocrystals Observed by Ultrafast Fluorescence Upconversion: The Effect of Surface Trap States. *J. Phys. Chem. C* **2008,** *112*, 12736–12746.
11. Garrett, M. D.; Bowers, M. J., II; McBride, J. R.; Orndorff, R. L.; Pennycook, S. J.; Rosenthal, S. J. Band Edge Dynamics in CdSe Nanocrystals Observed by Ultrafast Fluorescence Upconversion. *J. Phys. Chem. C* **2008,** *112*, 436–442.
12. Kippeny, T.; Bowers, M. J., II; Dukes, A. D., III; McBride, J. R.; Orndorff, R. L.; Garrett, M. D.; Rosenthal, S. J. Effects of Surface Passivation on the Exciton Dynamics of CdSe Nanocrystals as Observed by Ultrafast Fluorescence Upconversion Spectroscopy. *J. Chem. Phys.* **2008,** *128*, 1–8.
13. Underwood, D. F.; Kippeny, T.; Rosenthal, S. J. Ultrafast Carrier Dynamics in CdSe Nanocrystals Determined by Femtosecond Fluorescence Upconversion Spectroscopy. *J. Phys. Chem. B* **2001,** *105*, 436–443.

14. Makhal, A.; Yan, H.; Lemmens, P.; Kumar Pal, S. Light Harvesting Semiconductor Core−Shell Nanocrystals: Ultrafast Charge Transport Dynamics of CdSe−ZnS Quantum Dots. *J. Phys. Chem. C* **2010,** *114*, 627–632.
15. Underwood, D. F.; Kippeny, T.; Rosenthal, S. J. Charge Carrier Dynamics in CdSe Nanocrystals: Implications for the Use of Quantum Dots in Novel Photovoltaics. *Eur. Phys. J. D* **2001,** *16*, 241–244.
16. Bowers, M. J., II; McBride, J. R.; Garrett, M. D.; Sammons, J. A.; Dukes, A. D., III; Schreuder, M. A.; Watt, T. L.; Lupini, A. R.; Pennycook, S. J.; Rosenthal, S. J. Structure and Ultrafast Dynamics of White-Light-Emitting CdSe Nanocrystals. *J. Am. Chem. Soc.* **2009,** *131*, 5730–5731.
17. Klimov, V. I.; Schwarz, C. J.; McBranch, D. W.; Leatherdale, C. A.; Bawendi, M. G. Ultrafast Dynamics of Inter- and Intraband Transitions in Semiconductor Nanocrystals: Implications for Quantum-Dot Lasers. *Phys. Rev. B* **1999,** *60*, R2177–R2180.
18. Klimov, V. I.; Mikhailovsky, A. A.; McBranch, D. W.; LeatherdaleC. A.; Bawendi, M. G. Mechanisms for Intraband Energy Relaxation in Semiconductor Quantum Dots: The Role of Electron−Hole Interactions. *Phys. Rev. B* **2000,** *61*, R13349–R13352.
19. Guyot-Sionnest, P.; Shim, M.; Matranga, C.; Hines, M. Intraband Relaxation in CdSe Quantum Dots. *Phys. Rev. B* **1999,** *60*, R2181–R2184.
20. Burda, C.; Link, S.; Green, T. C.; El-Sayed, M. A. New Transient Absorption Observed in the Spectrum of Colloidal CdSe Nanoparticles Pumped with High-Power Femtosecond Pulses. *J. Phys. Chem. B* **1999,** *103*, 10775–10780.
21. Burda, C.; Link, S.; Mohamed, M. B.; El-Sayed, M. The Relaxation Pathways of CdSe Nanoparticles Monitored with Femtosecond Time-Resolution from the Visible to the IR: Assignment of the Transient Features by Carrier Quenching. *J. Phys. Chem. B* **2001,** *2001*, 12286–12292.
22. Cooney, R. R.; Sewall, S. L.; Dias, E. A.; Sagar, D. M.; Anderson, K. E. H.; Kambhampati, P. Unified Picture of Electron and Hole Relaxation Pathways in Semiconductor Quantum Dots. *Phys. Rev. B* **2007,** *75*, 1–14.
23. Shum, K.; Wang, W. B.; Alfano, R. R.; Jones, K. M. Observation of the 1P Excitonic States in Cd(S,Se)-Glass Quantum Dots. *Phys. Rev. Lett.* **1992,** *68*, 3904–3907.
24. Norris, D. J.; Sacra, A.; Murray, C. B.; Bawendi, M. G. Measurement of the Size Dependent Hole Spectrum in CdSe Quantum Dots. *Phys. Rev. Lett.* **1994,** *72*, 2612–2615.
25. Jones, M.; Lo, S. S.; Scholes, G. D. Signatures of Exciton Dynamics and Carrier Trapping in the Time-Resolved Photoluminescence of Colloidal CdSe Nanocrystals. *J. Phys. Chem. C* **2009,** *113*, 18632–18642.
26. McArthur, E. A.; Morris-Cohen, A. J.; Knowles, K. E.; Weiss, E. A. Charge Carrier Resolved Relaxation of the First Excitonic State in CdSe Quantum Dots Probed with Near-Infrared Transient Absorption Spectroscopy. *J. Phys. Chem. B* **2010,** *114*, 14514–14520.
27. Morris-Cohen, A. J.; Donakowski, M. D.; Knowles, K. E.; Weiss, E. A. The Effect of a Common Purification Procedure on the Chemical Composition of the Surfaces of CdSe Quantum Dots Synthesized with Trioctylphosphine Oxide. *J. Phys. Chem. C* **2010,** *114*, 897–906.
28. Morris-Cohen, A. J.; Frederick, M. T.; Lilly, G. D.; McArthur, E. A.; Weiss, E. A. Organic Surfactant-Controlled Composition of the Surfaces of CdSe Quantum Dots. *J. Phys. Chem. Lett.* **2010,** *1*, 1078–1081.
29. Burda, C.; Link, S.; Mohamed, M. B.; El-Sayed, M. The Pump Power Dependence of the Femtosecond Relaxation of CdSe Nanoparticles Observed in the Spectral Range from Visible to Infrared. *J. Chem. Phys.* **2002,** *116*, 3828–3833.
30. Zhang, J.; Zhang, X.; Zhang, J. Y. Size-Dependent Time-Resolved Photoluminescence of Colloidal CdSe Nanocrystals. *J. Phys. Chem. C* **2009,** *113*, 9512–9515.
31. De Mello Donega, C.; Koole, R. Size Dependence of the Spontaneous Emission Rate and Absorption Cross Section of CdSe and CdTe Quantum Dots. *J. Phys. Chem. C* **2009,** *113*, 6511–6520.
32. Klimov, V. I. Optical Nonlinearities and Ultrafast Carrier Dynamics in Semiconductor Nanocrystals. *J. Phys. Chem. B* **2000,** *104*, 6112–6123.
33. Germann, G. J.; Rakestraw, D. J. Multiplex Spectroscopy—Determining the Transition Moments and Absolute Concentrations of Molecular-Species. *Science* **1994,** *264*, 1750–1753.
34. Knowles, K. E.; Tice, D. B.; McArthur, E. A.; Solomon, G. C.; Weiss, E. A. Chemical Control of the Photoluminescence of CdSe Quantum Dot−Organic Complexes with a Series of *p*-Substituted Aniline Ligands. *J. Am. Chem. Soc.* **2010,** *132*, 1041–1050.
35. Koole, R.; Schapotschnikow, P.; De Mello Donega, C.; Vlugy, T. J. H.; Meijerink, A. Time-Dependent Photoluminescence Spectroscopy as a Tool To Measure the Ligand Exchange Kinetics on a Quantum Dot Surface. *ACS Nano* **2008,** *2*, 1703–1714.
36. Kalyuzhny, G.; Murray, R. W. Ligand Effects on Optical Properties of CdSe Nanocrystals. *J. Phys. Chem. B* **2005,** *109*, 7012–7021.
37. Munro, A. M.; Plante, I. J.-L.; Ng, M. S.; Ginger, D. S. Quantitative Study of the Effects of Surface Ligand Concentration on CdSe Nanocrystal Photoluminescence. *J. Phys. Chem. C* **2007,** *111*, 6220–6227.
38. Ji, X.; Copenhaver, D.; Sichmeller, C.; Peng, X. Ligand Bonding and Dynamics on Colloidal Nanocrystals at Room Temperature: The Case of Alkylamines on CdSe Nanocrystals. *J. Am. Chem. Soc.* **2008,** *130*, 5726–5735.
39. Bullen, C.; Mulvaney, P. The Effects of Chemisorption on the Luminescence of CdSe Quantum Dots. *Langmuir* **2006,** *22*, 3007–3013.
40. Qu, L.; Peng, X. Control of Photoluminescence Properties of CdSe Nanocrystals in Growth. *J. Am. Chem. Soc.* **2002,** *124*, 2049–2055.
41. Scott, A. M.; Miura, T.; Ricks, A. B.; Dance, Z. E. X.; Giacobbe, E. M.; Colvin, M. T.; Wasielewski, M. R. Spin-Selective Charge Transport Pathways through *p*-Oligophenylene-Linked Donor-Bridge-Acceptor Molecules. *J. Am. Chem. Soc.* **2009,** *131*, 17655–17666.